SEMI-ANNUAL PROGRESS REPORT

for

NASA GRANT NO. NAG-1-397

Period Covering 2/1/85-8/4/85

BRIDGMAN CRYSTAL GROWTH

by

Frederick M. Carlson
Mechanical & Industrial Engineering Department
Clarkson University
Potsdam, New York 13676

November 5, 1985

MODELING OF CONVECTION PHENOMENA IN BRIDGMAN-STOCKBARGER CRYSTAL GROWTH

Frederick M. Carlson, Arsev H. Eraslan and Ji-Zen Sheu

Clarkson University, Potsdam, New York 13676, U.S.A.

ABSTRACT

Thermal convection phenomena in a vertically oriented Bridgman-Stockbarger apparatus were modeled by computer simulations for different gravity conditions, ranging from earth conditions to extremely low gravity, approximate space conditions. The modeling results were obtained by the application of a state-of-the-art, transient, multi-dimensional, completely densimetrically coupled, discrete-element computational model which was specifically developed for the simulation of flow, temperature, and species concentration conditions in two-phase (solid-liquid) systems. The computational model was applied to the simulation of the flow and the thermal conditions associated with the convection phenomena in a modified Germanium-Silicon charge enclosed in a stationary fused-silica ampoule. The results clearly indicated that the gravitational field strength influences the characteristics of the coherent vortical flow patterns, interface shape and position, maximum melt velocity, and interfacial normal temperature gradient.

INTRODUCTION

It is well estrablished that melt convection exerts a strong influence on the processes that control the growth of compound semiconductor crystals. In Bridgman crystal growth, convection is driven by density differences in the melt which continuously interact with the local gravitational field. The majority of the problems encountered during attempts to produce homogeneous, defect-free crystals, are attributed to the direct result of melt convection through its influence on the heat and mass transport during solidification. Consequently, measures are usually taken to minimize convection and to enhance the possibility of crystal growth in a diffusion dominant regime. The microgravity environment of space offers excellent controlled laboratory conditions for studying the characteristics of the convection phenomenon in crystal growth which is simultaneously controlled by the density differences in the melt and the gravitational force field.

The physicochemical characteristics of crystals grown in space under microgravity conditions are usually quite different than their earth based counterparts grown under otherwise similar conditions. These differences however cannot be explained on the basis of the currently available mathematical models with analytic solutions (e.g., Sukanek, 1982; Lehoczky and Szofran, 1982), because their inherent simplifying assumptions usually tend to discard certain important details of the physical phenomena which control crystal growth. Order of magnitude studies (e.g., Camel and Favier, 1984) can also yield useful information, but again, generally lack the capability to consider the detailed consequences of the physical phenomena which are necessary to explain the different results of the experiments. Relatively simple, analytic or computational models which only consider diffusion (e.g., Coriell and Sekerka, 1979) are also usually inadequate in studies concerned with the understanding of the physics of crystal growth problems because they completely disregard the presence of the convection phenomenon which can strongly influence the solidification process.

The overall objective is to provide the required state-of-the-art computational modeling capability which can consider all the effects of the important physical phenomena, including convection and diffusion transport, body forces induced by

electromagnetic fields, Coriolis acceleration, and the acceleration due to transient motion, both under earth and microgravity space conditions. An important part of the overall objective is to understand the role of melt convection in crystal growth. Considering the fact that melt convection has not been established to be universally detrimental, a high level understanding of the physical phenomena can possibly provide a means of controlling convection, and hence, optimizing or improving the crystal growth process.

This study presents the results of the preliminary applications of the computational model to the simulation of crystal growth in a stationary cylindrical ampoule, under axially symmetric, thermally driven flow conditions, without any solutal convection, and with the gravitational force aligned with the vertical ampoule axis. The results are presented for sytematically varying gravitational field strength conditions, and for typical furnace conditions, in order to illustrate the effects of the gravity field on the crystal growth process in a relatively well controlled Bridgman system.

SUMMARY OF DISCRETE-ELEMENT COMPUTATIONAL MODEL

The discrete-element method (DEM) (e.g., Eraslan, 1974; Eraslan, Lin and Sharp, 1982; Eraslan and Lin, 1985; Eraslan 1985) directly utilizes the integral-forms of the physical principles in the development of the spatially discretized computational systems for the solutions of the velocity, temperature and species mass-fraction (concentration) conditions, by identically satisfying the conservation principle for melt mass in each and every "element". Since, it does not require any consideration of the continuum-limit partial differential equations (i.e., continuity equation, Navier-Stokes equation, energy equation, etc.), associated with the formulations of the conventional mathematical models, the DEM is conceptually and mathematically different than the finite-difference method (FDM) and the finite-element method (FEM); and it is similar (only conceptually) to classical fluid-in-cell (FLIC) and integrated-finite-difference (box) direct numerical simulation methods [e.g., Gentry, Martin and Daly, 1966; Harlow and Amsden, 1969; Roache, 1972).

Composite-Space-Splitting Algorithm

The application of the three-dimensional DEM to the simulation of the convection and diffusion phenomena in crystal growth considers a special discretization form, in cylindrical coordinates (r,θ,z), which utilizes four partially overlapping half-elements, in the (r,θ) plane, in each element. Two half-elements are used for the computation of the r-component of velocity, and two half-elements are used for the computation of the θ-component of velocity, in each element. The three-dimensional method calculates (1) the melt free-surface elevation in N elements of the surface layer, (2) the r-component of velocity in 2N half-elements, (3) the θ-component of velocity in 2N half-elements, (4) the z-component of velocity on N enclosure surfaces, (5) the pressure on N enclosure surfaces, (6) the temperature in N elements, and (7) the species mass-fractions (concentrations) in N elements of the computational region. The complete computational system of 7(seven) sets of spatially dicretized equations for elements ($i=1,2,\ldots,I$; $j=1,2,\ldots,J$; $\ell=1,2,\ldots,L$) can be represented as

$$\frac{\partial h}{\partial t}_{i,j} = [\text{discrete-element equations for melt-surface elevation in the elements of the surface layer } (\ell=L)],$$

$$\frac{\partial V}{\partial t}_{r;i\pm\frac{1}{2},j,\ell} = [\text{discrete-element equations for r-component of velocity in the 2(two) half-elements of the internal layers}],$$

$\frac{\partial V_{\theta;i,j\pm\frac{1}{2},\ell}}{\partial t}$ = [discrete-element equations for θ-component of velocity in the 2(two) half-elements of the internal layers],

$V_{z;i,j,\ell+\frac{1}{2}}$ = [discrete-element equations for z-component of velocity at the enclosure surfaces, between the internal layers of the elements],

$P_{i,j,\ell-\frac{1}{2}}$ = [discrete-element equations for pressure at the enclosure surfaces between the internal layers of the elements].

$\frac{\partial T_{i,j,\ell}}{\partial t}$ = [discrete-element equations for temperature in the elements],

$\frac{\partial C_{k;i,j,\ell}}{\partial t}$ = [discrete-element equations for species mass-fraction (concentration) in the elements].

The discrete-element system is formulated by considering spatially discretized forms of the phenomenological parts, represented as (1) "flow" for melt mass transport in the conservation of mass equation, (2) "conv" for "convection" transport in all equations, (3) "forc" for "pressure force" and "body force" (including the "gravity force" and the "Coriolis force") in all momentum equations, (4) "visc" for "viscous stress" in all momentum equations, (5) "cond,k" for "thermal conduction" in the energy equation, (6) "diff,D" for "mass diffusion" in the species-mass-conservation equations, and (7) "genr" for "generation" in the energy and species-mass-conservation equations.

Composite-Time-Splitting Algorithm

Timewise numerical integration of the DEM model is based on a novel, explicit computational algorithm which uses the composite-time-splitting technique. The numerical integration advances the solution in time by considering (1) a single-step, two-time-level partial algorithm for the calculations of "conv", the convection transport terms, which guarantees the elimination of the first-order numerical dispersion effects, and (2) a two-step, three-time-level partial algorithm for the calculations of "forc", the force terms, "visc", "cond,k", diff,D", the nonconvective transport terms, and "genr", the generation terms.

With the known solution set at the initial time t^n, the composite-time-splitting algorithm of timewise numerical integration can be represented in the generalized difference operator notation for the phenomenological parts.

At the intermediate time level $t^{n+\frac{1}{2}} = t^n + \gamma_t \Delta t^n$:

(1) melt-surface elevation h,

$$h^{n+\frac{1}{2}}_{i,j} = h^n_{i,j} + \gamma_t \Delta t^n \left[\Delta^n_{flow} h\right]^n_{i,j,L} + \gamma_t \Delta t^n \left[\frac{1}{(1+\beta)} \left(\frac{\partial \beta}{\partial t}\right) \Delta \bar{z}\right]^n_{i,j,L} \qquad (1)$$

(2) r-component of velocity V_r ,

$$V^{n+\frac{1}{2}}_{r;i\pm\frac{1}{2},j,\ell} = V^n_{r;i\pm\frac{1}{2},j,\ell} + \gamma_t \Delta t^n \left[\Delta^n_{conv} V_r\right]^n_{i\pm\frac{1}{2},j,\ell}$$

$$+ \gamma_t \Delta t^n \left[\Delta^n_{forc} V_r\right]^n_{i\pm\frac{1}{2},j,\ell} + \gamma_t \Delta t^n \left[\Delta^n_{visc} V_r\right] \qquad (2)$$

(3) θ-component of velocity V_θ,

$$V^{n+\frac{1}{2}}_{\theta;i,j\pm\frac{1}{2},\ell} = V^{n}_{\theta;i,j\pm\frac{1}{2},\ell} + \gamma_t \Delta t^n \left[\Delta^n_{conv} V_\theta\right]^n_{i,j\pm\frac{1}{2},\ell}$$

$$+ \gamma_t \Delta t^n \left[\Delta^n_{forc} V_\theta\right]^n_{i,j\pm\frac{1}{2},\ell} + \gamma_t \Delta t^{-1} \left[\Delta^n_{visc} V_\theta\right]^n_{i,j\pm\frac{1}{2},\ell} \qquad (3)$$

(4) temperature T,

$$T^{n+\frac{1}{2}}_{i,j,\ell} = T^{n}_{i,j,\ell} + \gamma_t \Delta t^n \left[\Delta^n_{conv} T\right]^n_{i,j,\ell} + \gamma_t \Delta t^n \left[\Delta^n_{cond,\varepsilon} T\right]^n_{i,j,\ell}$$

$$+ \gamma_t \Delta t^n \left[\Delta^n_{genr} \dot{q}\right]^n_{i,j,\ell} \qquad (4)$$

(5) mass-fraction (concentration) C_k of species-k:

$$C^{n+\frac{1}{2}}_{k;i,j,\ell} = C^{n}_{k;i,j,\ell} + \gamma_t \Delta t^n \left[\Delta^n_{conv} C_k\right]^n_{i,j,\ell} + \gamma_t \Delta t^n \left[\Delta^n_{diff,D} C_k\right]^n_{i,j,\ell}$$

$$+ \gamma_t \Delta t^n \left[\Delta^n_{genr} \dot{C}_k\right]^n_{i,j,\ell} \qquad (5)$$

(6) z-component of velocity V_z,

$$V^{n+\frac{1}{2}}_{z;i,j,\ell+\frac{1}{2}} = V^{n+\frac{1}{2}}_{z;i,j,\ell-\frac{1}{2}} + \left[\Delta^{n+\frac{1}{2}}_{flow} V_z\right]^{n+\frac{1}{2}}_{i,j,\ell} + \left[\frac{1}{(1+\beta)} \left(\frac{\partial \beta}{\partial t}\right) \Delta \bar{z}\right]^{n+\frac{1}{2}}_{i,j,\ell} \qquad (6)$$

(7) pressure p,

$$p^{n+\frac{1}{2}}_{i,j,\ell-\frac{1}{2}} = p^{n+\frac{1}{2}}_{i,j,\ell+\frac{1}{2}} + \left[\left(\frac{\partial V_z}{\partial t}\right) \Delta \bar{z}\right]^{n+\frac{1}{2}}_{i,j,\ell} + \left[\Delta^{n+\frac{1}{2}}_{conv} V_z\right]^{n}_{i,j,\ell}$$

$$+ \left[\Delta^{n+\frac{1}{2}}_{forc} V_z\right]^{n+\frac{1}{2}}_{i,j,\ell} + \left[\Delta^{n+\frac{1}{2}}_{visc} V_z\right]^{n+\frac{1}{2}}_{i,j,\ell} \qquad (7)$$

at the solution (final) time level $t^{n+1} = t^n + \Delta t^n$:

(1) melt-surface elevation h,

$$h^{n+1}_{i,j} = h^{n}_{i,j} + \Delta t^n \left[\Delta^{n+\frac{1}{2}}_{flow} h\right]^{n+\frac{1}{2}}_{i,j,L} + \Delta t^n \left[\frac{1}{(1+\beta)} \left(\frac{\partial \beta}{\partial t}\right) \Delta \bar{z}\right]^{n+\frac{1}{2}}_{i,j,L} \qquad (8)$$

(2) r-component of velocity V_r,

$$V^{n+1}_{r;i\pm\frac{1}{2},j,\ell} = V^{n}_{r;i\pm\frac{1}{2},j,\ell} + \Delta t^n \left[\Delta^{n+\frac{1}{2}}_{conv} V_r\right]^{n}_{i\pm\frac{1}{2},j,\ell}$$

$$+ \Delta t^n \left[\Delta^{n+\frac{1}{2}}_{forc} V_r\right]^{n+\frac{1}{2}}_{i\pm\frac{1}{2},j,\ell} + \Delta t^n \left[\Delta^{n+\frac{1}{2}}_{visc} V_r\right]^{n+\frac{1}{2}}_{i\pm\frac{1}{2},j,\ell} \qquad (9)$$

(3) θ-component of velocity V_θ,

$$V^{n+1}_{\theta;i,j\pm\frac{1}{2},\ell} = V^{n}_{\theta;i,j\pm\frac{1}{2},\ell} + \Delta t^n \left[\Delta^{n+\frac{1}{2}}_{conv} V_\theta\right]^n_{i,j\pm\frac{1}{2},\ell}$$

$$+ \Delta t^n \left[\Delta^{n+\frac{1}{2}}_{forc} V_\theta\right]^{n+\frac{1}{2}}_{i,j\pm\frac{1}{2},\ell} + \Delta t^n \left[\Delta^{n+\frac{1}{2}}_{visc} V_\theta\right]^{n+\frac{1}{2}}_{i,j\pm\frac{1}{2},\ell} \qquad (10)$$

(4) temperature T,

$$T^{n+1}_{i,j,\ell} = T^{n}_{i,j,\ell} + \Delta t^n \left[\Delta^{n+\frac{1}{2}}_{conv} T\right]^{n+\frac{1}{2}}_{i,j,} + \Delta t^n \left[\Delta^{n+\frac{1}{2}}_{cond,\varepsilon} T\right]^{n+\frac{1}{2}}_{i,j,\ell}$$

$$+ \Delta t^n \left[\Delta^{n+\frac{1}{2}}_{genr} \dot{q}\right]^{n+\frac{1}{2}}_{i,j,\ell} \qquad (11)$$

(5) mass-fraction (concentration) C_K of species-k:

$$C^{n+1}_{k;i,j,\ell} = C^{n}_{k;i,j,\ell} + \Delta t^n \left[\Delta^{n+\frac{1}{2}}_{conv} C_k\right]^{n+\frac{1}{2}}_{i,j,\ell} + \Delta t^n \left[\Delta^{n+\frac{1}{2}}_{diff,D} C_k\right]^{n+\frac{1}{2}}_{i,j,\ell}$$

$$+ \Delta t^n \left[\Delta^{n+\frac{1}{2}}_{genr} \dot{C}_k\right]^{n+\frac{1}{2}}_{i,j,\ell} \qquad (12)$$

(6) z-component of velocity V_z,

$$V^{n+1}_{z;i,j,\ell+\frac{1}{2}} = V^{n+1}_{z;i,j,\ell-\frac{1}{2}} + \left[\Delta^{n+\frac{1}{2}}_{flow} V_z\right]^{n+1}_{i,j,\ell} \left[\frac{1}{(1+\beta)} \left(\frac{\partial \beta}{\partial t}\right) \Delta \bar{z}\right]^{n+1}_{i,j,\ell} \qquad (13)$$

(7) pressure p,

$$p^{n+1}_{i,j,\ell-\frac{1}{2}} = p^{n+1}_{i,j,\ell+\frac{1}{2}} + \left[\left(\frac{\partial V_z}{\partial t}\right) \Delta \bar{z}\right]^{n+\frac{1}{2}}_{i,j,\ell} + \left[\Delta^{n+1}_{conv} V_z\right]^{n}_{i,j,\ell}$$

$$+ \left[\Delta^{n+1}_{forc} V_z\right]^{n+1}_{i,j,\ell} + \left[\Delta^{n+1}_{visc} V_z\right]^{n+1}_{i,j,\ell} \qquad (14)$$

Phenomenological Parts of the Difference Operators

The spatially discretized phenomenological parts of the difference operators in Eqs. (1) through (14) are formulated, according to the composite-space-splitting algorithm of the DEM, at the two time levels, t^n and $t^{n+\frac{1}{2}}$, of the composite-time-splitting algorithm.

Abbreviated forms of the "flow" difference operator for the melt-surface elevation at the initial time level t^n and at the intermediate time level $t^{n+\frac{1}{2}}$, respectively, can be represented as:

$$\left[\Delta^{n}_{flow} h\right]^{n}_{i,j} = \text{Eq. (15b), with } n+\tfrac{1}{2} \text{ replaced by } n, \qquad (15a)$$

$$[\Delta^{n+\frac{1}{2}}_{flow} h]^{n+\frac{1}{2}}_{i,j} = \frac{1}{A_{z,i,j}(1 + \beta^{n+\frac{1}{2}}_{i,j,L})} [\tilde{G}_{\beta;i-\frac{1}{2},j,L} - \tilde{G}_{\beta;i+\frac{1}{2},j,L}$$

$$+ \text{additional flow terms for melt mass transport}]. \qquad (15b)$$

Abbreviated forms of the "conv" difference operator for the r-component of velocity at the initial time level t^n and at the intermediate time level $t^{n+\frac{1}{2}}$, respectively, can be represented as:

$$[\Delta^{n}_{conv} V_r]^{n}_{r-\frac{1}{2},j,\ell} = \text{Eq. (16b), with } n+\tfrac{1}{2} \text{ replaced by } n, \qquad (16a)$$

$$[\Delta^{n+\frac{1}{2}}_{conv} V_r]^{n}_{i-\frac{1}{2},j,\ell} = \frac{1}{\bar{V}^{n+\frac{1}{2}}_{i-\frac{1}{2},j,\ell}(1 + \bar{\beta}^{n+\frac{1}{2}}_{i-\frac{1}{2},j,\ell})} [\bar{\tilde{G}}^{n+\frac{1}{2}}_{\beta,r;i-\frac{1}{2},j,\ell} (\tilde{V}^{n}_{r;i-\frac{1}{2},j,\ell} - V^{n}_{r;i-\frac{1}{2},j,\ell})$$

$$- G^{n+\frac{1}{2}}_{\beta,r;i,j,\ell} (\tilde{V}^{n}_{r;i,j,\ell} - V^{n}_{r;i-\frac{1}{2},j,\ell})$$

$$+ \text{additional convective transport terms}] \qquad (16b)$$

Abbreviated forms of the "forc" difference operator for the r-component of velocity at the initial time level t^n and at the intermediate time level $t^{n+\frac{1}{2}}$, respectively, can be represented as:

$$[\Delta^{n}_{forc} V_r]^{n}_{i-\frac{1}{2},j,\ell} = \text{Eq. (17b), with } n+\tfrac{1}{2} \text{ replaced by } n, \qquad (17a)$$

$$[\Delta^{n+\frac{1}{2}}_{forc} V_r]^{n+\frac{1}{2}}_{i-\frac{1}{2},j,\ell} = \frac{1}{\bar{V}^{n+\frac{1}{2}}_{i-\frac{1}{2},j,\ell}(1 + \bar{\beta}^{n+\frac{1}{2}}_{i-\frac{1}{2},j,\ell})} [\bar{\bar{A}}^{n+\frac{1}{2}}_{r;i=\frac{1}{2},j,\ell} (\bar{p}^{n+\frac{1}{2}}_{i-\frac{1}{2},j,\ell} - p^{n+\frac{1}{2}}_{i-\frac{1}{2},j,\ell})$$

$$- \bar{A}^{n+\frac{1}{2}}_{r;i,j,\ell} (\bar{p}^{n+\frac{1}{2}}_{i,j,\ell} - \bar{p}^{n+\frac{1}{2}}_{i-\frac{1}{2},j,\ell})$$

$$+ \text{additional pressure terms}] + g^{n+\frac{1}{2}}_{a} \cos\theta^{n+\frac{1}{2}}_{N,r}$$

$$+ \Omega^{n+\frac{1}{2}}_{\theta;i-\frac{1}{2},j,\ell} V^{n+\frac{1}{2}}_{z;i-\frac{1}{2},j,\ell} - \Omega^{n+\frac{1}{2}}_{z;i-\frac{1}{2},j,\ell} \bar{V}^{n+\frac{1}{2}}_{\theta;i-\frac{1}{2},j,\ell} \qquad (17b)$$

Abbreviated forms of the "visc" difference operator for the r-component of velocity at the initial time level t^n and at the intermediate time level $t^{n+\frac{1}{2}}$, respectively, can be represented as:

$$[\Delta^{n}_{visc} V_r]^{n}_{i-\frac{1}{2},j,\ell} = \text{Eq. (18b), with } n+\tfrac{1}{2} \text{ replaced by } n, \qquad (18a)$$

$$[\Delta^{n+\frac{1}{2}}_{visc} V_r]^{n+\frac{1}{2}}_{i-\frac{1}{2},j,\ell} = \frac{1}{\bar{V}^{n+\frac{1}{2}}_{i-\frac{1}{2},j,\ell}\,(1 + \bar{\beta}^{n+\frac{1}{2}}_{i-\frac{1}{2},j,\ell})}$$

$$\cdot\,[\bar{A}^{n+\frac{1}{2}}_{r;i-\frac{1}{2},j,\ell}\,\bar{\sigma}^{n+\frac{1}{2}}_{\nu,rr;i-\frac{1}{2},j,\ell} - \bar{A}^{n+\frac{1}{2}}_{r;i,j,\ell}\,\bar{\sigma}^{n+\frac{1}{2}}_{\nu,rr;i,j,\ell}$$

$$+ \text{additional viscous stress terms } (\sigma_{\nu,rr},\ \sigma_{\nu,\theta r},\ \sigma_{\nu,zr})] \qquad (18b)$$

The spatially discretized phenomenological parts of the difference operators in Eqs. (1) through (14) for (1) the θ-component of velocity, (2) the pressure (from the z-component of the momentum equation), (3) the temperature, and (4) the mass-fraction (concentration) of species-k are also formulated, according to the composite-space-splitting algorithm of the DEM, at the two time levels, t^n and $t^{n+\frac{1}{2}}$, of the composite-time-splitting algorithm.

The enclosure surface areas A_r, A_θ and A_z and the volumes v of the elements and half-elements, used in the formulations of the difference operators, Eqs. (16a) through (18b), are formulated according to the spatial discretization of the DEM in cylindrical coordinates (r,θ,z), i.e.,

$$A_r = r\Delta\theta\Delta\bar{z},\quad A_\theta = \Delta r\Delta\bar{z},\quad \bar{A}_z = r\Delta\theta\Delta r,\quad \bar{v} = r\Delta\theta\Delta r\Delta\bar{z}\ . \qquad (19)$$

The DEM formulation of the computational model considers the mathematical system as completely densimetrically coupled, in the sense that the density variations, with temperature and species mass-fractions, are retained exactly in all the terms of the governing discrete-element equations. Therefore, the DEM model does not resort to the use of the simplifying Boussinesq approximation (e.g., Eraslan, Lin and Sharp, 1982); but it considers the variations of the density in terms of the generalized compressibility fraction β defined as

$$\rho = \rho_o\,(1 + \frac{\Delta\rho}{\Delta\rho_o}) = \rho_o\,(1 + \beta) \qquad (20)$$

such that the directional flow rates across the enclosure surfaces of the elements and half-elements explicitly include the local effects of compressibility, i.e.,

$$\tilde{\bar{G}}_{\beta,r} = r\Delta\theta\Delta\bar{z}\,\bar{V}_r\,(1 + \beta);\quad \tilde{\bar{G}}_{\beta,\theta} = \Delta r\Delta\bar{z}\,\bar{V}_\theta\,(1 + \beta);\quad \tilde{\bar{G}}_{\beta,z} = r\Delta\theta\Delta r\,V_z(1 + \tilde{\beta}) \qquad (21)$$

The general abbreviated forms of the "conv" difference operator, associated with convective transport for the solution temperature T and species mass-fraction (concentration) C_k, at two time levels, can be expressed as

$$[\Delta^n_{conv} F]^n_{i,j,\ell} = \text{Eq. (22b), with } n+\tfrac{1}{2} \text{ replaced by } n, \qquad (22a)$$

$$[\Delta^{n+\frac{1}{2}}_{conv} F]^n_{i,j,\ell} = \frac{1}{\bar{V}^{n+\frac{1}{2}}_{i,j,\ell}(1 + \beta^{n+\frac{1}{2}}_{i,j,\ell})}\,[G^{n+\frac{1}{2}}_{\beta,r;i-\frac{1}{2},j,\ell}\,(\tilde{F}^n_{i-\frac{1}{2},j,\ell} - F^n_{i,j,\ell})$$

$$+\tilde{\bar{G}}^{n+\frac{1}{2}}_{\beta,r;i+\frac{1}{2},j,\ell}\,(\tilde{F}^n_{i+\frac{1}{2},j,\ell} - F^n_{i,j,\ell})$$

$$+ \text{additional convective transport terms } (F)] \qquad (22b)$$

It is important to point out that the special form of the convective transport term, formulated as the difference between the value of the flow variable at the enclosure surface and its computational value in the element or half-element, represents a new intensive-form (IF), which introduces more desirable stability characteristics to the numerical solutions.

Directional-Transportive-Upwind-Interpolation (DTUI)

The general computational algorithm of the discrete-element method (DEM) incorporates the directional-transportive-upwind-interpolation (DTUI) technique which represents a second-order formulation, based on (1) half-point velocity components at the enclosure surfaces of the elements and half-elements and (2) the specified time step of numerical integration. The second-order upwind-differencing technique evaluates the transported values of the intensive flow properties at specific locations upstream of the enclosure surface as they move with the flow during the specified time period, i.e.,

$$\tilde{r}_{i-\frac{1}{2},j,\ell} = r_{i-\frac{1}{2},j,\ell} + \tilde{\Delta r}_{i-\frac{1}{2},j,\ell} = r_{i-\frac{1}{2},j,\ell} - \alpha_t \Delta t \, \bar{V}_{r;i-\frac{1}{2},j,\ell} \tag{23a}$$

$$\tilde{\theta}_{i-\frac{1}{2},j,\ell} = \theta_{i-\frac{1}{2},j,\ell} + \tilde{\Delta\theta}_{i-\frac{1}{2},j,\ell} = \theta_{i-\frac{1}{2},j,\ell} - \alpha_t \Delta t \, \bar{V}_{\theta;i-\frac{1}{2},j,\ell} \tag{23b}$$

$$\tilde{z}_{i-\frac{1}{2},j,\ell} = \bar{z}_{i-\frac{1}{2},j,\ell} + \tilde{\Delta z}_{i-\frac{1}{2},j,\ell} = \bar{z}_{i-\frac{1}{2},j,\ell} - \alpha_t \Delta t \, \bar{V}_{z;i-\frac{1}{2},j,\ell} \tag{23c}$$

where,

$$\alpha_t = 0.5 - 0.6 \text{ (depending on the stability characteristics).} \tag{24}$$

With the evaluated, directional-transportive-upwind locations, Eqs. (23a), (23b) and (23c), the computational algorithm uses the multi-dimensional-interpolation (MDI) algorithm to evaluate the directional-transportive-upwind values of all the fluid properties at the transport enclosure surface, by using the values of the fluid properties in all the adjacent elements and/or half-elements.

As examples, the MDI forms of the DTUI values of the r-component of velocity and the temperature or species mass-fraction (concentration) can be represented as

$$\tilde{V}_{r;i-\frac{1}{2},j,\ell} = \mathrm{MDI}\left[V_r(\tilde{r}_{i-\frac{1}{2},j,\ell}, \tilde{\theta}_{i-\frac{1}{2},j,\ell}, \tilde{z}_{i-\frac{1}{2},j,\ell}; V_{r;i-\frac{1}{2},(i-1)+\frac{1}{2};j,j\pm1;\ell,\ell\pm1})\right] \tag{25a}$$

$$\tilde{F}_{i-\frac{1}{2},j,\ell} = \mathrm{MDI}\left[F(\tilde{r}_{i-\frac{1}{2},j,\ell}, \tilde{\theta}_{i-\frac{1}{2},j,\ell}, \tilde{z}_{i-\frac{1}{2},j,\ell}; F_{i,i-1;j,j\pm1;\ell,\ell\pm1})\right] \tag{25b}$$

Discussions of Convergence (Consistency, Stability, Accuracy)

The composite-space-time-splitting, with directional-transportive-upwind-interpolation and multi-dimensional-interpolation, (CSTS-DTUI-MDI) algorithm tends to eliminate all the nonphysical contributions of the numerical dispersion (computationally generated) effects to the transport. The application of the heuristic stability technique (e.g., Roache, 1972) to the linear model systems, representing the identical wave, convection and diffusion phenomena establishes that the convergence of the (CSTS-DTUI-MDI) algorithm to the partial differential equations

(PDE) is of accuracy order Δt^2 (Δt square) in the time step for each of the phenomenological terms, provided that all the required stability criteria, (1) Courant-Friedrichs-Lewy (CFL), based on the surface wave speed for maximum melt depth D_m, (2) Courant, based on the maximum velocity V_{max} in the melt, and (3) Neumann, based on the maximum diffusivity ϵ_{max} in the solid and/or in the melt, are met, i.e.,

$$\frac{\Delta t\,(g_a\,D_{max})^{\frac{1}{2}}}{2\,\min(\Delta r, r\Delta\theta, \Delta z)} \leq 1 \tag{26a}$$

$$\frac{\Delta t\,V_{max}}{2\,\min(\Delta r, r\Delta\theta, \Delta z)} \leq 1 \tag{26b}$$

$$\frac{\Delta t\,\max(\epsilon_{max})}{[\min(\Delta r, r\Delta\theta, \Delta z]^2} \leq 1 \tag{26c}$$

It is important to point out that the stability of the CSTS-TDUI-MDI algorithm is completely independent of all the considerations of the characteristic numbers, including Prandtl, Schmidt, and Grashof numbers. The expanded limit of the discrete-element system converges directly to the standard transient three-dimensional PDE system, with the additional error terms that can be represented in the form of higher-order-derivative (HOD) terms, i.e.,

continuity equation:

$$\frac{\partial \rho}{\partial t} - \frac{1}{r}\frac{\partial}{\partial r}(r\rho V_r) + \frac{1}{r}\frac{\partial}{\partial \theta}(\rho V_\theta) + \frac{\partial}{\partial z}(\rho V_z)$$

$$= \Delta t\ \mathrm{HOD}\left[\left(\tfrac{1}{2}\text{-}\gamma_t\right) F\left(\frac{\partial^{m+n}}{\partial r^m \partial \theta^n}, \frac{\partial^{m+n}}{\partial r^m \partial z^n}, \frac{\partial^{m+n}}{\partial \theta^m \partial z^n}\ ;\ m+n = 2\right)\right]$$

$$+ \Delta t^2\ \mathrm{HOD}\left[F\left(\frac{\partial^{m+n}}{\partial r^m \partial \theta^n}, \frac{\partial^{m+n}}{\partial r^m \partial z^n}, \frac{\partial^{m+n}}{\partial \theta^m \partial z^n}\ ;\ m+n > 2\right)\right] \tag{27}$$

r-component of the Navier-Stokes (N-S) equation

$$\frac{\partial}{\partial t}(\rho V_r) - \frac{1}{r}\frac{\partial}{\partial r}(r\rho V_r V_r) + \frac{1}{r}\frac{\partial}{\partial \theta}(\rho V_\theta V_r) - \frac{\rho}{r}V_\theta^{\,2} + \frac{\partial}{\partial z}(\rho V_z V_r)$$

$$= -\frac{\partial p}{\partial r} + \frac{1}{r}\frac{\partial}{\partial r}(r\sigma_{\nu,rr}) + \frac{1}{r}\frac{\partial \sigma_{\nu,\theta r}}{\partial \theta} - \frac{\sigma_{\nu,\theta\theta}}{r} + \frac{\partial \sigma_{\nu,zr}}{\partial z}$$

$$- g_a \rho \cos\theta_{N,r} + \rho\left(\Omega_{cor,N,\theta} V_z - \Omega_{cor,N,z} V_\theta\right)$$

$$+ \Delta t\ \mathrm{HOD}\left[\left(\tfrac{1}{2}\text{-}\gamma_t\right) F\left(\frac{\partial^{m+n}}{\partial r^m \partial \theta^n}, \frac{\partial^{m+n}}{\partial r^m \partial z^n}, \frac{\partial^{m+n}}{\partial \theta^m \partial z^n}\ ;\ m+n = 2\right)V_r\right]$$

$$+ \Delta t^2\ \mathrm{HOD}\left[F\left(\frac{\partial^{m+n}}{\partial r^m \partial \theta^n}, \frac{\partial^{m+n}}{\partial r^m \partial z^n}, \frac{\partial^{m+n}}{\partial \theta^m \partial z^n}\ ;\ m+n > 2\right)V_r\right] \tag{28}$$

Each of the remaining DEM equations also converges to the appropriate PDE with Δt^2 order accuracy in the time step.

It is important to point out that in all DEM equations, the selection of the value of the parameter γ_t, for determining the intermediate time level $t^{n+1/2}$, as

$$\gamma_t = 0.5 - 0.6 \text{ (depending on the stability characteristics).} \quad (29)$$

results in the elimination of the Δt-order terms in Eqs. (27), (28) and all other PDE equations. Therefore, the CSTS-DTUD-MDI algorithm tends to eliminate all the numerical dispersion effects in the solution of the DEM computational model; and hence, it can be classified as a consistent and stable (i.e., convergent) algorithm with second-order convergent accuracy in time step Δt.

Consideration of the Solid and Melt Subregions and Modeling of the Phase Change at the Interface

The DEM model utilizes the same computational algorithm for the calculations of the solutions in both the melt and solid subregions of the entire region of the charge, by considering two different marker values for identifying each element as containing either solid (marker = 0) or melt (marker = 1, as liquid). The computational algorithm changes the marker value in an element only as a consequence of the phase change conditions in the element, according to a kinetic phase-change submodel. The phase change phenomenon (solidification or melting) is formulated by considering the solidification (melting) temperature and the phase diagram of the charge, and the local temperature and species mass-fraction (concentration) distributions along the solid-melt interface, which are controlled by the overall heat transfer and mass transport conditions of the crystal growth experiment. The special formulations of the DEM computational model and the kinetic phase-change submodel eliminate the need to consider different numerical solutions for the solid and melt subregions, and more importantly, eliminate the need to match conditions at the solid-melt interface as a moving boundary.

APPLICATION TO A TYPICAL BRIDGMAN-STOCKBARGER EXPERIMENT

The outlined DEM computational model was applied to the simulation of a typical Bridgman -Stockbarger crystal growth experiment for studying the convection phenomenon under varying gravitational field strength conditions.

Description of the Apparatus

An ampoule, insulated on both its top and bottom, is placed in the middle of a furnace which has a large adiabatic zone (Fig. 1). The hot and cold zones are arranged such that parts of the ampoule wall can be maintained at approximately constant temperature levels above and below the charge melting point. The ampoule is made of fused silica, with 0.185 cm thick walls, an outer diameter of 1.805 cm, and an overall length of 7.6192 cm. The stationary ampoule contains a charge similar to a Germanium-Silicon compound, except that the solutal coefficient of volume expansion has been set equal to zero. Because the charge contracts upon solidification, the top of the melt is not held in contact with the ampoule, but it is allowed to behave as a free surface, which closely simulates the actual processing conditions. Thermophysical properties of the system are also given in Fig. 1.

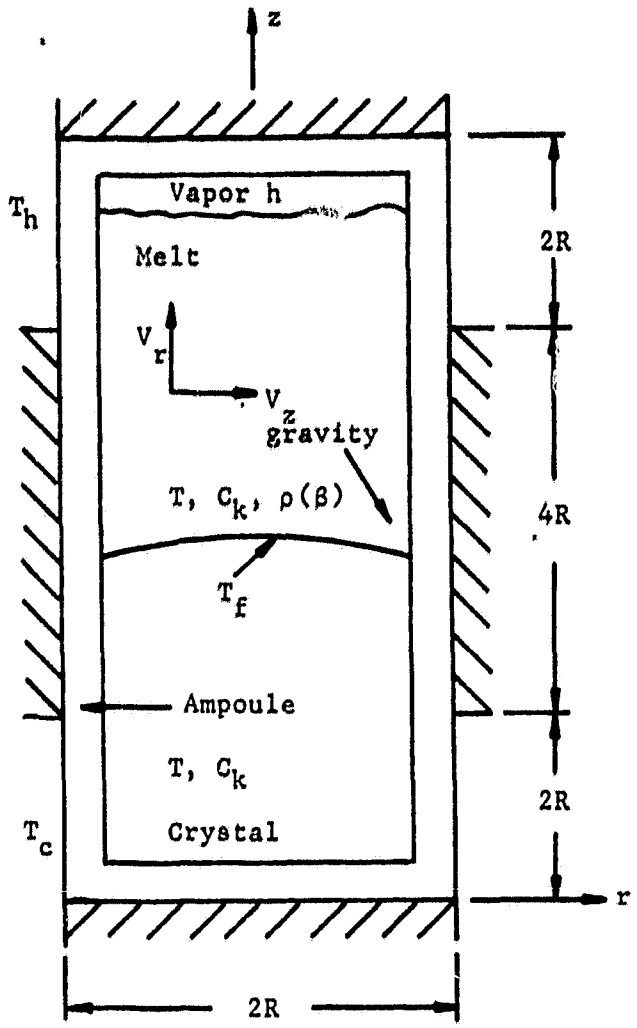

C = 0.39 Cal/g·k
specific heat
d = 0.185 cm
ampoule wall thickness
f = f(r) cm
interface equation
$g_a = g_e - 10^{-8}g_e$ (g_e = 9.8 m/s^2)
gravitational acceleration
L = 7.6192 cm
ampoule length
Pr = 5.88 (10^{-3})
Prandtl number
R = 0.9525 cm
ampoule outside radius
Tc = 765°C
cooler temperature
T_f = 937°C
solidification temperature
T_h = 1070°C
heater temperature
β_T = 5.0 (10^{-4})/°K
thermal coefficient of volume expansion
ε_a = 0.1247 cm^2/s
ampoule thermal diffusivity
ε_m = 0.1870 cm^2/s
melt thermal diffusivity
ε_c = 0.0815 cm^2/s
crystal thermal diffusivity
ρ = 5.48 g/cm^3
charge density
ν = 1.10 (10^{-3}) cm^2/s
kinematic viscosity

Fig. 1. Schematic of a Bridgman-Stockbarger System and Thermophysical Properties.

Description of the Computer Simulations

In preliminary applications of the general, transient, three-dimensional DEM Computational model to the described simulation of the Bridgman-Stockbarger crystal growth experiment, it was assumed that the direction of the gravitational field was aligned with the vertical axis of the ampoule. Furthermore, it was assumed that the the axial symmetry conditions could be maintained under all applied vertical gravitational force fields.

The computer simulations were started with an arbitrary, but realistic, solid-melt interface location and shape in the ampoule. For a specified gravitational field strength, the transient computer simulations were continued until steady-state conditions were attained both for the location and shape of the interface, and for the coherent recirculation patterns of the convection cells in the melt.

Discussion of Results

The gravitational field strength was allowed to vary from $1.0g_e$ to $10^{-8}g_e$ in four steps. The flow fields resulting from this systematic variation are presented in Figs. 2-5 in which only half of the r-z plane is shown. The strongest circulation at

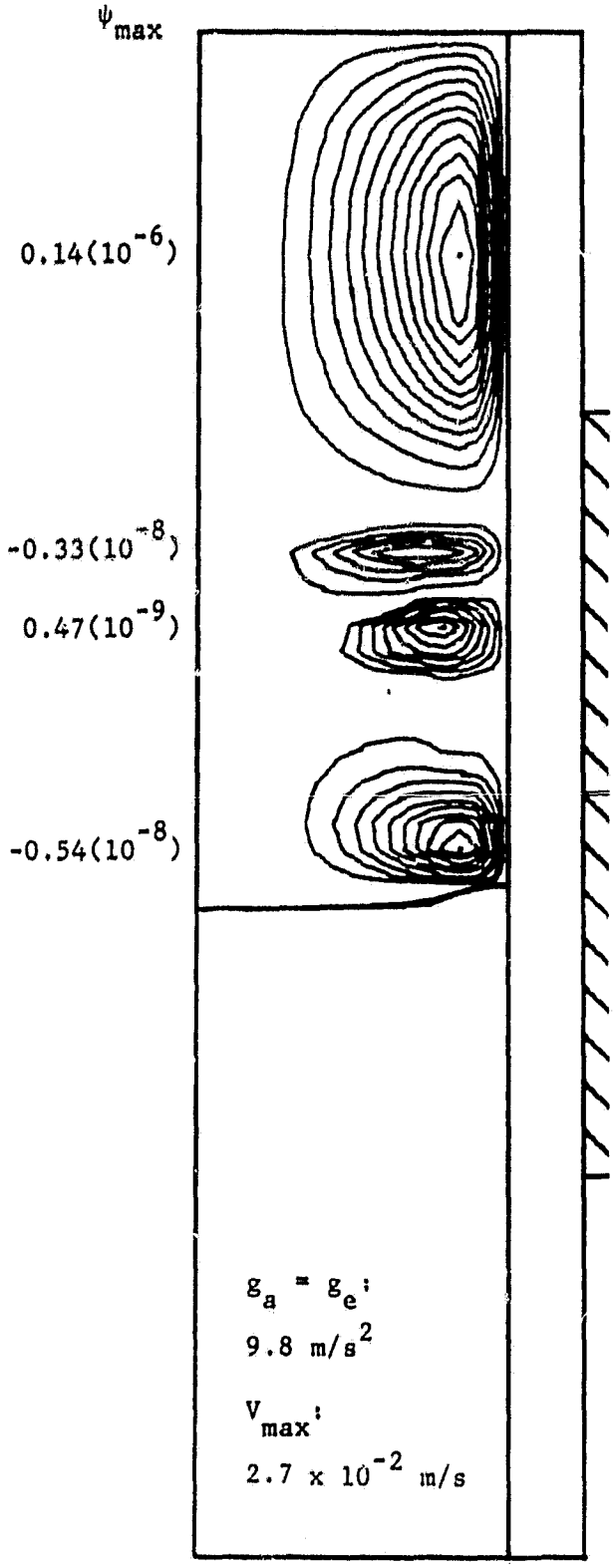

Fig. 2. Streamline Representation of Melt Convection Flow Cells
Gravity Field: $1.0g_e$.

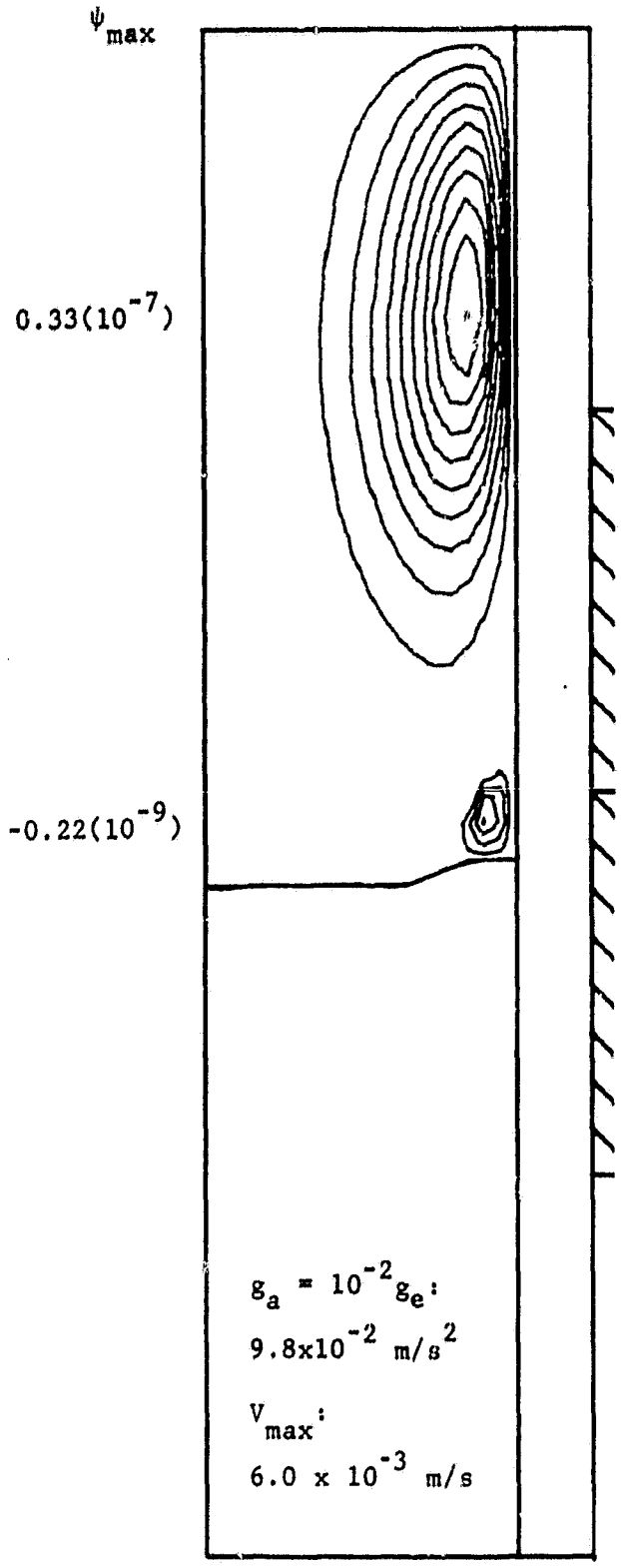

Fig. 3. Streamline Representation of Melt Convection Flow Cells
Gravity Field: $10^{-2}g_e$.

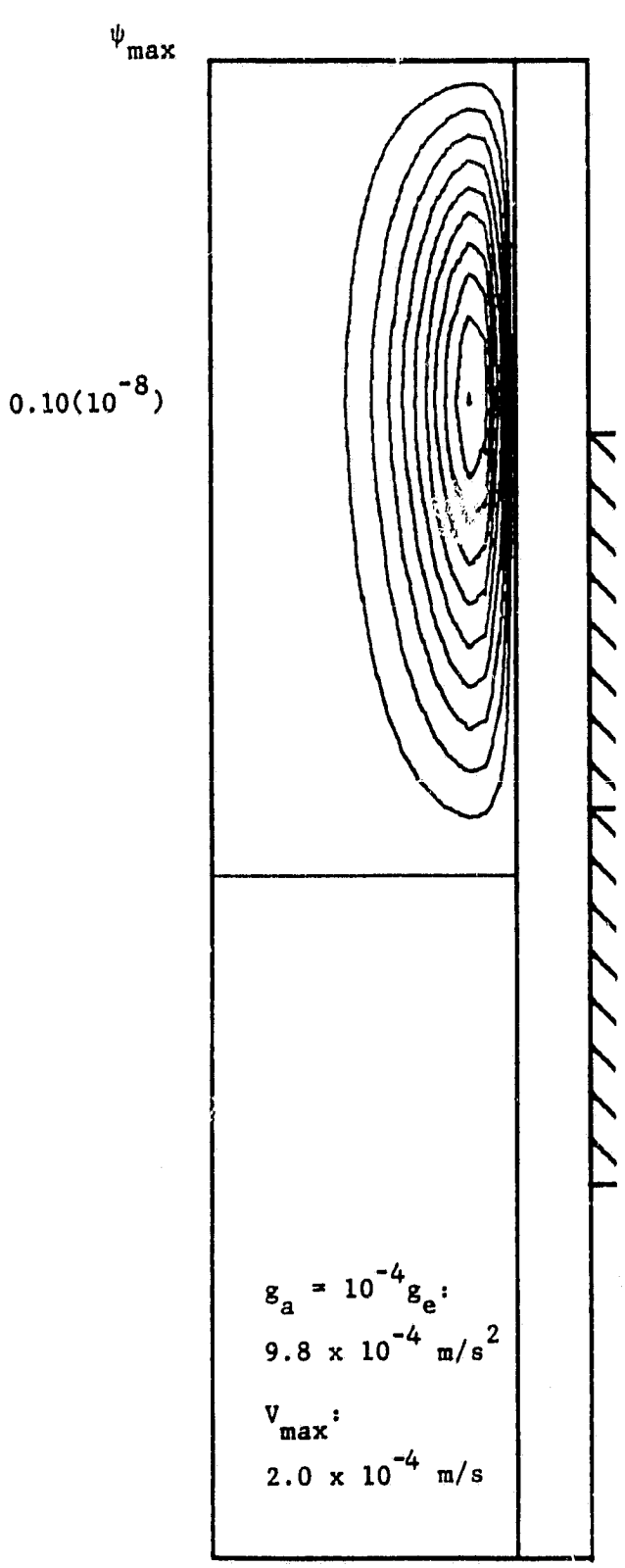

Fig. 4. Streamline Representation of Melt Convection Flow Cells
Gravity Field: $10^{-4} g_e$.

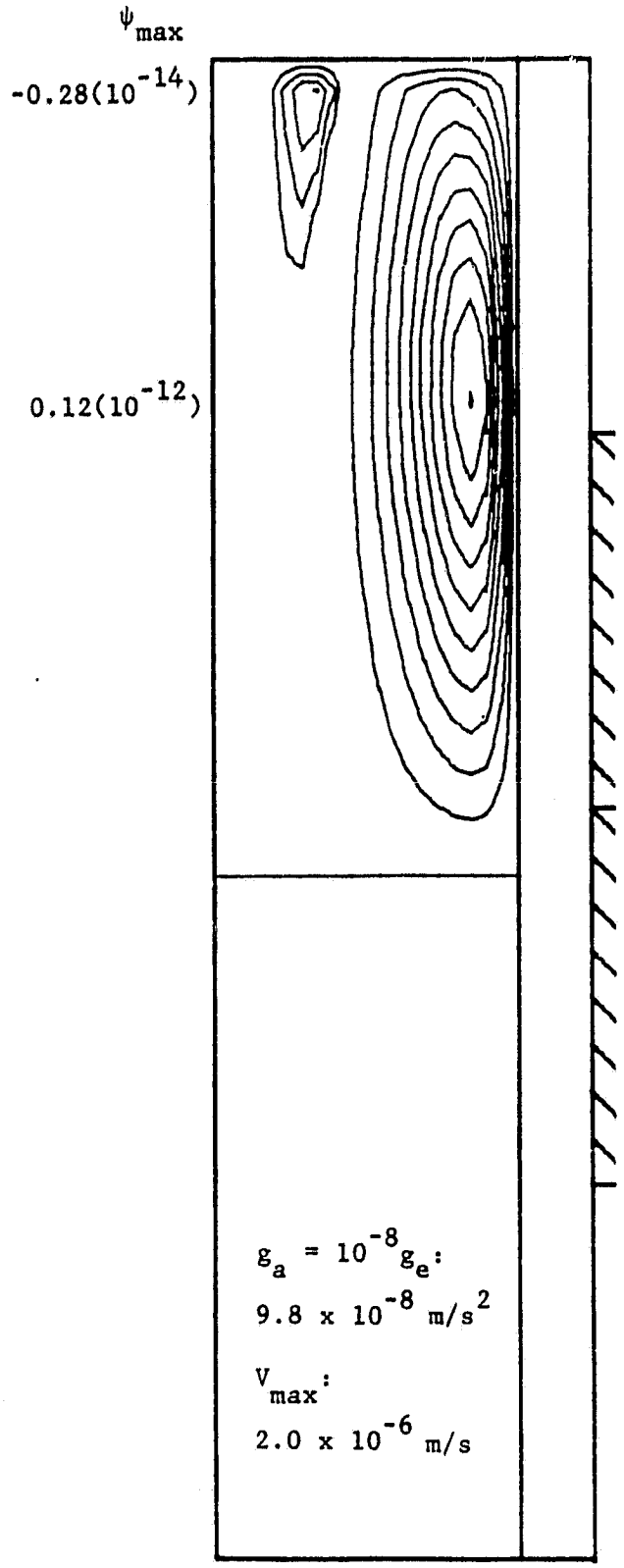

Fig. 5. Streamline Representation of Melt Convection Flow Cells
Gravity Field: $10^{-8} g_e$.

any gravitational level is always in the largest cell which is adjacent to the wall in the vicinity of the heater zone. Cell circulation is counterclockwise with the flow upward along the wall, as denoted by the positive value of streamfunction ψ. The center of any cell is the maximum value of ψ for that cell. Equal ψ increments are then shown between the center of each cell and the zero value on the ampoule wall. Adjacent cells always rotate in opposite directions.

As gravity decreases, both the quantative and qualitative nature of the flow and transport change. Four cells decrease to one and then increase again to two, but the nature of the flow has changed in the process. The horizontally stratified cells of Fig. 2 give way to the unicellular flow of Fig. 4 which in turn yields to the vertical cell pattern of Fig. 5. This could have a substantial influence on the transport process if the transport equation is convection dominated. Semiconductor melts typically have Prandtl and Schmidt numbers on the order of 0.01 and 100.0, respectively. Consequently, while rather vigorous convection will be necessary to affect heat transport, species transport is altered at much lower melt velocities. Thus, while the species distribution is nearly uniform within the cells of Fig. 2, species transport between cells is by diffusion making the horizontally stratified field considerably different than the vertical field.

Figure 6, a plot of the interface for various gravity levels, shows that convection has no influence on interface shape or location at intensities less than $10^{-4}g_e$. At higher levels the interface progressively moves downward into the cold zone and changes shape. A recent publication (Carlson, Fripp, and Crouch, 1984) has shown that changing the sign of the interface curvature radically alters the flow field. While not shown, it has been calculated that the convective component of the energy transport is only 15% of the total transport at $1.0g_e$, 5% at $10^{-2}g_e$, and approximately zero elsewhere.

Constitutional supercooling is important in multicomponent melts. Increasing fluid motion increases the interfacial normal temperature gradient, as indicated in Fig. 7. The bulk fluid is more thoroughly mixed and hence a higher temperature gradient appears near the interface. Again no influence is felt at gravitational levels below $10^{-4}g_e$ where conduction dominates. Fluid motion thus diminishes the chances for constitutional supercooling to occur.

CONCLUSIONS AND RECOMMENDATIONS

The convection phenomenon in Bridgmann-Stockbarger experiments, under varying gravitational force conditions, was simulated by using a computational model. The results of the preliminary applications of the computational model indicated that, as expected, if gravitational force conditions can be reduced, the melt convection phenomenon can also be reduced significantly in the crystal growth experiment.

However, the preliminary applications did not consider various important effects which exist under reduced gravity conditions, including (1) the effect of reduced melt convection on the species mass transport in the charge, (2) the effect of enhanced Coriolis acceleration (force), (3) the effect of enhanced surface tension, and (4) the effects of sudden acceleration or deceleration, that could result from orbital control requirements. Considering the cost of space projects, it is important to take into account all these important effects in the design and planning of the crystal growth experiments for future missions. Therefore, a state-of-the-art, transient, three-dimensional computational model can be recommended as a cost-effective design tool for simulating crystal growth experiments under realistic and detailed microgravity conditions that would exist in actual orbital stations.

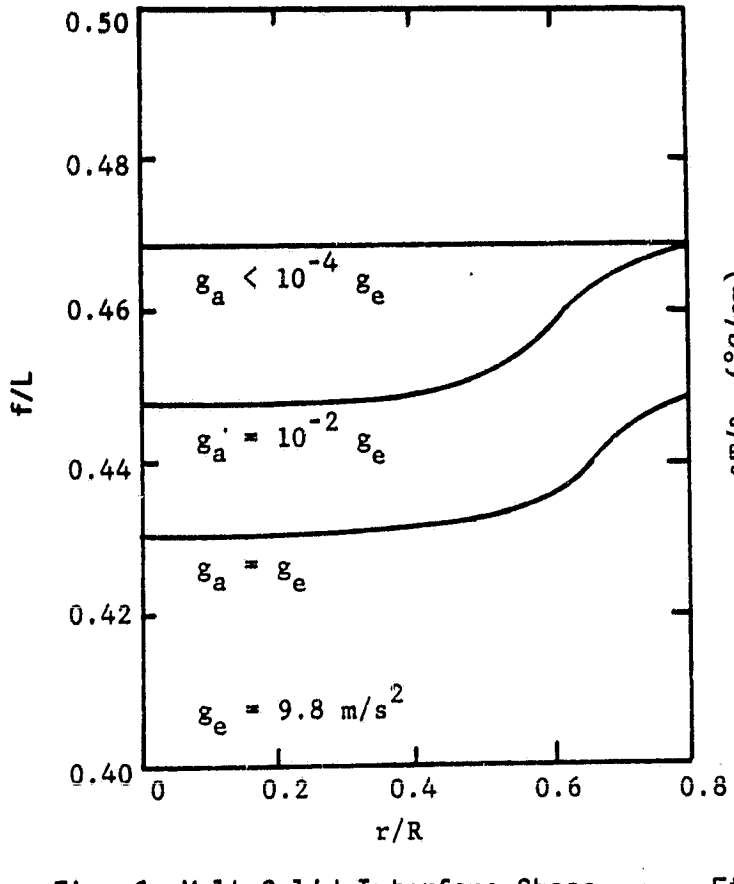

Fig. 6. Melt-Solid Interface Shape for Various Gravitational Field Strength Conditions.

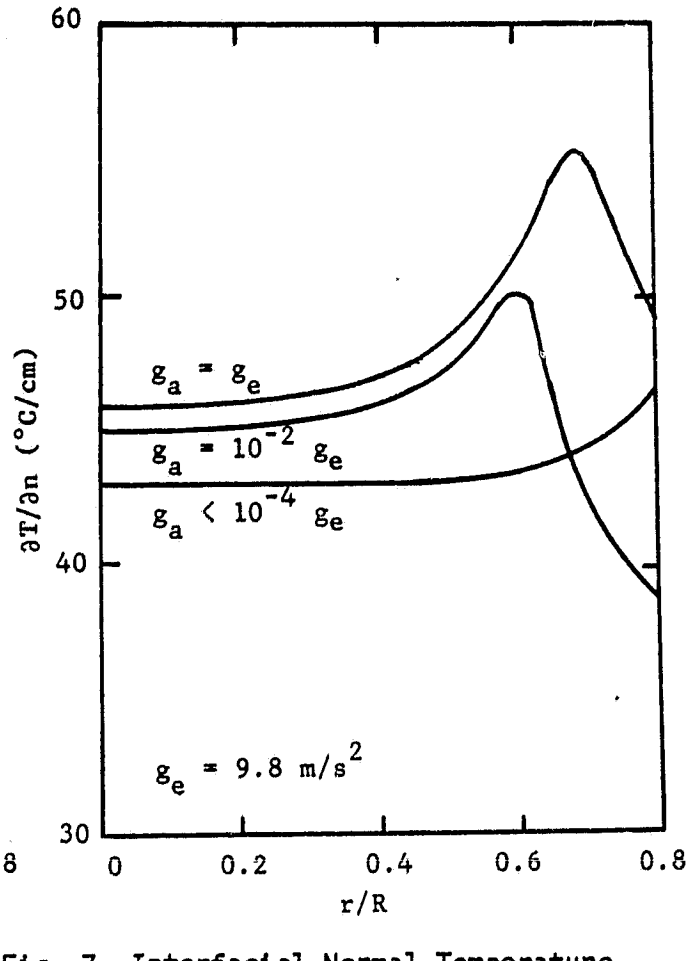

Fig. 7. Interfacial Normal Temperature Gradient for Various Gravitational Field Strength Conditions.

ACKNOWLEDGMENT

This research was partially sponsored by the National Aeronautics and Space Administration under Grant NAG-1-397.

REFERENCES

Camel, D. and J. J. Favier (1984). Thermal Convection and Longitudinal Macrosegregation in Horizontal Bridgman Crystal Growth. J. Crystal Growth, 67, 42-56.

Carlson, F. M., A. L. Fripp, and R. K. Crouch (1984). Thermal Convection During Bridgman Crystal Growth. J. Crystal Growth, 68, 747-756.

Clayton, J. C., M. C. Davidson, D. C. Gillies, and S. L. Lehoczky (1982). One Dimensional Analysis of Segregation in Directionally Solidified HgCdTe. J. Crystal Growth, 60, 374-380.

Coriell, S. R. and R. F. Sekerka (1979). Lateral Solute Segregation During Unidirectional Solidification of a Binary Alloy With a Curved Solid-Liquid Interface J. Crystal Growth, 46, 479-482.

Eraslan, A. H. (1975). A Transient, Two-Dimensional Discrete-Element Model for Far-Field Analysis of Thermal Discharges in Coastal Regions. In J. A. Schetz (Ed.) Progress in Astronautics and Aeronautics, vol. 36, AIAA Publications, New York. pp. 165-201.

Eraslan, A. H., W. L. Lin, and R. D. Sharp (1983). FLOWER: A Computer Code for

Simulating Three-Dimensional Flow, Temperature and Salinity Conditions in Rivers, Estuaries and Coastal Regions. NUREG/CR-3172, U.S. Nuclear Regulatory Commission, Office of Nuclear Regulatory Research, Washington, D.C.

Eraslan, A. H. (1985). A Second-Order Algorithm for Fast-Transient Multi-Dimensional Computational Fluid Dynamics. 38th Meeting, American Physical Society, Division of Fluid Dynamics, Tuscon, Arizona.

Gentry, R. A., R. E. Martin, and B. J. Daly (1966) An Eulerian Differencing Method for Unsteady Compressible Flow Problem. J. Comput. Phys. 1, pp. 87-118, 1966.

Harlow, F. H., and A. A. Amsden, Fluid Dynamics: An Introductory Text, LA-4281, Los Alamos National Laboratory, Los Alamos, N.M., 1969.

Lehoczky, S. L. and F. R. Szofran (1982). Directional Solidification and Characterization of HgCdTe Alloy. In G. E. Rindone (Ed.), Materials Processing in the Reduced Gravity Environment of Space, vol. 9, North Holland, pp. 409-420.

Roache, P. J., Computational Fluid Dynamics, Hermosa Publishers, Albuquerque, New Mexico, 1972.

Sukanek, P. C. (1982). Deviation of Freezing Rate From Translation Rate in the Bridgman-Stockbarger Technique. J. Crystal Growth, 58, 208-228.